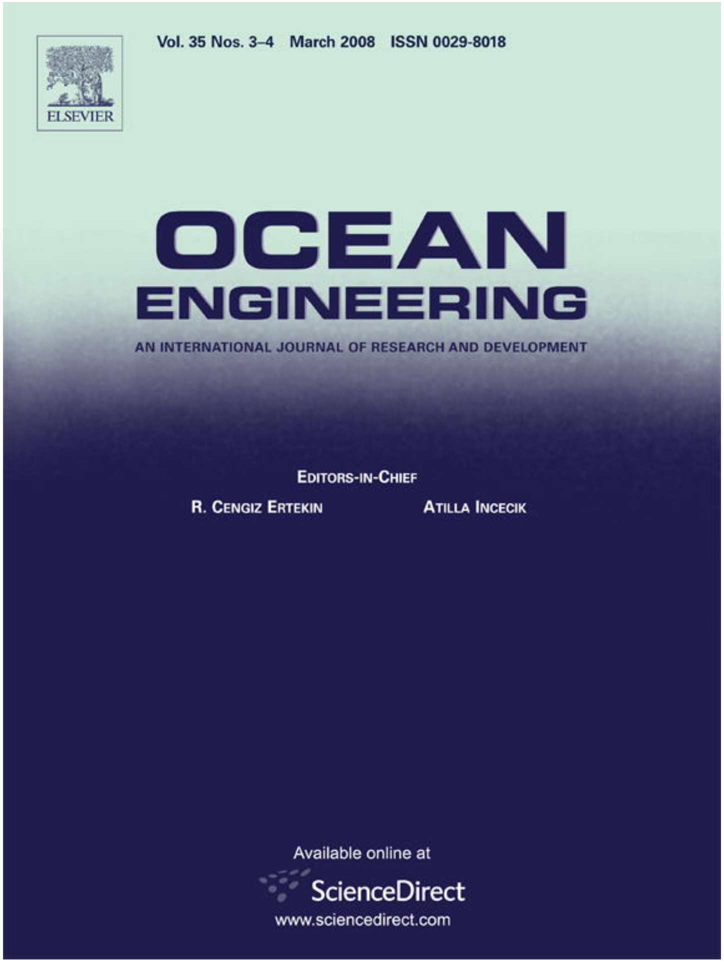
Vol. 35 Nos. 3–4 March 2008 ISSN 0029-8018
ELSEVIER
OCEAN
ENGINEERING
AN INTERNATIONAL JOURNAL OF RESEARCH AND DEVELOPMENT
EDITORS-IN-CHIEF
R. CENGIZ ERTEKIN
ATILLA INCECIK
Available online at
ScienceDirect
www.sciencedirect.com

Available online at www.sciencedirect.com
ScienceDirect
Ocean Engineering 35 (2008) 367–379
OCEAN ENGINEERING
www.elsevier.com/locate/oceaneng

# Surface gravity waves from direct numerical simulations of the Euler equations: A comparison with second-order theory

A. Toffoli[a,*], M. Onorato[b], E. Bitner-Gregersen[a,*], A.R. Osborne[b], A.V. Babanin[c]

[a]*Det Norske Veritas, Veritasveien 1, Høvik 1322, Norway*
[b]*Dip. Fisica Generale, Universitá di Torino, Via P. Giuria 1, 10125 Torino, Italy*
[c]*Faculty of Engineering and Industrial Sciences, Swinburne University of Technology, P.O. Box 218, Hawthorn, Victoria 3122, Australia*

Received 2 July 2007; accepted 10 October 2007
Available online 13 October 2007

**Abstract**

When the wave spectrum is sufficiently narrow-banded and the wave steepness is sufficiently high, the modulational instability can take place and waves can be higher than expected from second-order wave theory. In order to investigate these effects on the statistical distribution of long-crested, deep water waves, direct numerical simulations of the Euler equations have been performed. Results show that, for a typical design spectral shape, both the upper and lower tails of the probability density function for the surface elevation significantly deviate from the commonly used second-order wave theory. In this respect, the crest elevation is observed to increase up to 18% at low probability levels. It would furthermore be expected that wave troughs become shallower due to nonlinear effects. Nonetheless, the numerical simulations show that the trough depressions tend to be deeper than in second-order theory.


*Keywords:* Euler equations; High-order nonlinearity; Long-crested waves; Nonlinear waves; Second-order theory; Wave crest distribution; Wave trough distribution

## 1. Introduction

The wave amplitude represents an important wave characteristic for many practical applications. For the design of marine structures, for example, the statistical distribution of the crest elevation (i.e., the highest elevation of an individual wave) must be established with care as it is an input to wave load calculations. Further, for offshore platforms a proper statistical knowledge of extreme crests are essential for defining a sufficient air gap under a platform deck to ensure that a wave crest does not endanger the structure integrity. Also the distribution of wave troughs (i.e., the deepest depression of an individual wave) is of significance for engineering applications. For example, it is essential for the definition of the maximal trough depth in the design of offshore rigs, because underwater cross-bars must not be exposed to the air, but at the same time should be sufficiently close to the surface. A proper statistical description of wave trough, moreover, is important for the definition of tether loads for the design of tension-leg platforms.

As a first approximation, the water surface can be represented as a Gaussian random process (linear wave theory). Provided the wave spectrum is narrow-banded and the phases of the Fourier components are uniformly distributed, the probability distribution of linear wave crests and troughs follows the Rayleigh distribution (see Longuet-Higgins, 1952). Real waves, however, are different than linear theory would predict. The wave crests are actually higher and sharper while the wave troughs are shallower and flatter than in a Gaussian process (see, for example, Ochi, 1998, and reference therein). As a result, the statistical distribution of crests and troughs deviates from the Rayleigh distribution.

In order to capture such effects, it is common practice to approximate the surface elevation by including the second-order, bound, contribution for each free wave mode

*Corresponding authors. Tel.: +47 67577261; fax: +47 67579911.
*E-mail addresses:* alessandro.toffoli@dnv.com, toffoli.alessandro@gmail.com (A. Toffoli), elzbieta.bitner-gregersen@dnv.com (E. Bitner-Gregersen).

0029-8018/$ - see front matter © 2007 Elsevier Ltd. All rights reserved.
doi:10.1016/j.oceaneng.2007.10.004

(i.e., second-order wave theory: Hasselmann, 1962; Longuet-Higgins, 1963). Exploration of this approach has revealed that statistical properties of random, unidirectional, narrow-band, second-order wave trains agree relatively well with wave measurements (see, e.g., Forristall, 2000; Prevosto et al., 2000, among others). Nonetheless, there are wave records that clearly show a large discrepancy between measurements of crest amplitudes and second-order theory, especially in the extreme tail of the distribution (see, e.g., Bitner-Gregersen and Magnusson, 2004; Petrova et al., 2006).

Second-order theory, in this respect, only accounts for bound (i.e., phase locked) modes, and hence does not involve the nonlinear interaction between free waves. For certain spectral conditions, it has been shown that the latter can also be responsible for significant deviation from Gaussian statistics (Janssen, 2003; Onorato et al., 2004; Socquet-Juglard et al., 2005; Mori and Janssen, 2006). This departure can be attributed to the Benjamin–Feir instability mechanism, which, for irregular waves, can take place when the wave spectrum is sufficiently narrow and the steepness is sufficiently high. Janssen (2003), in particular, demonstrated that the statistical properties of long-crested, deep water waves strongly depend on the ratio between the wave steepness and the spectral bandwidth (see also Mori and Janssen, 2006), which is referred to as the Benjamin–Feir index (BFI); note that this parameter, with a different name, was already proposed by Onorato et al. (2001).

To take the effects of both bound and free waves into account, the statistical properties of nonlinear wave trains have been investigated by means of direct numerical simulations of the primitive Euler equations (see, for example, Brandini, 2001; Mori and Yasuda, 2002) as well as flume experiments (Onorato et al., 2004, 2006). Provided the BFI is sufficiently large, results have shown that the deviation from the Gaussian statistics can be more significant than in second-order theory. Recently, similar findings have also been discussed by Gibson et al. (2007), who have investigated the wave crest distribution by combining a fully nonlinear wave model with reliability methods, which are used for design and safety assessment of marine structures.

In the present study, we use Monte Carlo simulations of the Euler equations to perform a systematic analysis of the differences between the statistical properties of fully nonlinear long-crested waves and second-order long-crested waves. Both wave crest and wave trough distributions are taken into account. The paper is organized as follows. We first begin with a brief description of the numerical methods and the simulation technique. In Section 4, the statistical properties of the surface elevation simulated with the Euler equations are compared with the values expected in second-order theory. We show, in particular, that free wave modes have significant effects on the occurrence of extreme values in agreement with theoretical (Janssen, 2003; Mori and Janssen, 2006) and experimental (Onorato et al., 2004) results. This leads to a deviation of the tails of the probability density function. In this respect, nonlinear effects are expected to increase the crest height and decrease the trough depression. However, whereas the crest elevations are observed to exceed the second-order prediction, we will show that the wave troughs are actually deeper than in second-order profiles. In the section following that, the probability distributions of crest and trough amplitudes are shown; changes of the shape of the distribution are discussed as a function of the BFI. The statistical distribution of the trough-to-crest wave height is also discussed. In Section 6, the distribution of extremes is computed from the crest, trough, and trough-to-crest height distributions; the occurrence of extreme amplitudes is then discussed as a function of the number of events. Conclusions will be reported in the last section.

## 2. Theoretical methods

In the case of constant water depth ($h=\infty$ in this study), the velocity potential $\phi(x,z,t)$ of an irrotational, inviscid, and incompressible liquid that propagates in one ($x$) direction satisfies the Laplace's equation everywhere in the fluid (see, for example, Whitham, 1974). The boundary conditions are such that the vertical velocity at the bottom ($z=-\infty$) is zero, and the kinematic and dynamic boundary conditions are satisfied for the velocity potential $\psi(x,t)=\phi(x,\eta(x,t),t)$ on the free surface, i.e., $z=\eta(x,t)$ (see Zakharov, 1968); the expressions of the kinematic and dynamic boundary conditions are as follows:

$$\eta_t+\psi_x\eta_x-W[1+(\eta_x)^2]=0, \tag{1}$$

$$\psi_t+g\eta+\tfrac{1}{2}(\psi_x)^2-\tfrac{1}{2}W^2[1+(\eta_x)^2]=0, \tag{2}$$

where the subscripts denote the partial derivatives; $W(x,t)$ represents the vertical velocity evaluated at the free surface.

It is straightforward to show that a first-order (linear) solution of the governing equations for irregular waves takes the following form (Whitham, 1974):

$$\eta^{(1)}(x,t)=\sum_{i=1}^{N}a_i\cos(k_ix-\omega_it+\varepsilon_i), \tag{3}$$

where $t$ is time, $x$ the position, $k_i$ the wavenumber, and $\omega_i$ the angular frequency, which is related to the wavenumber through the linear dispersion relation $\omega_i=\sqrt{gk_i}$; $\varepsilon_i$ is a uniformly distributed random phase in $[0,2\pi]$; $N$ is the total number of frequencies; $a_i$ is a Rayleigh-distributed random amplitude (see, e.g., Prevosto, 1998) with

$$\langle a_i^2\rangle=\langle a(k_i)^2\rangle=2E(k_i)\Delta k, \tag{4}$$

where $\langle\cdot\rangle$ refers to the expected value, and $E(k_i)$ is the spectral density function in wavenumber space.

A second-order correction to the linear wave surface (Eq. (3)) was first derived for deep water by Longuet-

Higgins (1963); it has the following form:

$$\eta^{(2)}(x,t) = \frac{1}{4}\sum_{i,j=1}^{N} a_i a_j [K_{ij}^{-}\cos(\varphi_i - \varphi_j) + K_{ij}^{+}\cos(\varphi_i + \varphi_j)], \tag{5}$$

where $\varphi_i = k_i x - \omega_i t + \varepsilon_i$, and $K_{ij}^{+}$ and $K_{ij}^{-}$ are the coefficients of the sum and difference contributions.

The expression reported in Eq. (5) only involves the contribution of bound waves up to the second-order. Nonlinear terms higher than the third-order are considered negligible and hence excluded. In order to achieve a more complete description of the wave field, which includes nonlinear interactions higher than third-order as well as the effects related to the dynamics of free wave modes, direct numerical simulations of Eqs. (1) and (2) can be performed. To this end, different numerical approaches can be found in the literature; a review is presented in Tsai and Yue (1996). Recently new, promising methods have been proposed by Annenkov and Shrira (2001), Clamond and Grue (2001), Zakharov et al. (2002). For this study, we have used the high-order spectral method (HOSM), which was proposed independently by Dommermuth and Yue (1987) and West et al. (1987); a concise review of HOSM can also be found in Tanaka (2001a). A comparison of the two methods has recently been presented by Clamond et al. (2006). Their results indicate that the formulation proposed by Dommermuth and Yue (1987) does not converge when the amplitude is very small unlike the formulation by West et al. (1987). The latter, therefore, has been chosen for the present study.

HOSM uses a series expansion in the wave slope of the vertical velocity $W(x,t)$ about the free surface; herein we have considered a third-order expansion so that the four-wave interaction is included (see Tanaka, 2001b). This expansion is used to evaluate the velocity potential $\phi(x,\eta(x,t),t)$ and the surface elevation $\eta(x,t)$ from Eqs. (1) and (2) at each instant of time. All aliasing errors generated in the nonlinear terms are removed (see Tanaka, 2001a, for details). The time integration is then performed by means of a four-order Runge–Kutta method. A small time-step, $\Delta t = 0.02\,\mathrm{s}$, is used to minimize the energy leakage; throughout the simulations, the variation of total energy remains lower than 0.5%.

## 3. Numerical experiments

For irregular wave trains, the crest distribution can be obtained from the analysis of many random simulations of the sea surface. In the case of second-order wave theory, the nonlinear sea surface at a certain time $t$ can be calculated from Eqs. (3) and (5) as follows: $\eta(x,t) = \eta^{(1)}(x,t) + \eta^{(2)}(x,t)$. For a certain input spectral condition, repetitions have been performed by using different random phases and random amplitudes; approximately 60 000 waves have been simulated.

In the case the Euler equations are used, records of the sea surface can be obtained by the evolution of Eqs. (1) and (2); the input surface $\eta(x,t=0)$ is computed with Eq. (3); the velocity potential $\psi(x,t=0)$ is then obtained from the input surface by using linear wave theory (see, e.g., Whitham, 1974). The total duration of the computation is 200 $T_p$; using a 2.4 GHz processor, the computation requires about 3.5 min of CPU time. The output surfaces $\eta(x,t)$ are captured every three times $T_p$, after the statistical properties of the surface elevation have stabilized. To ensure enough samples for the statistical analysis, many repetitions ($\approx 500$) have been performed with different initial surfaces (i.e., different random phases and random amplitudes). For consistency with the second-order experiment, 60 000 individual waves have been considered for the analysis.

As it is frequently used for many practical applications, the JONSWAP formulation (see, for example, Komen et al., 1994) is herein used to define several input frequency spectra. An expression in the wavenumber space can be obtained using the linear dispersion relation (see Tanaka, 2001a). The input spectra are defined with 256 equally spaced wavenumbers; the spacial domain is chosen such that the wave field measures 1410 m.

Input spectral densities are generated considering a constant dominant wavelength $\lambda_p = 156\,\mathrm{m}$ (which correspond to a peak period $T_p = 10\,\mathrm{s}$), and different values of the Phillips parameter $\alpha$ and peak enhancement factor $\gamma$. Although, $\alpha$ and $\gamma$ are not free parameters in a natural environment (Babanin and Soloviev, 1998), we select their values in order to generate slightly different sea states, where the significant wave height is kept constant and the spectral energy is gradually concentrated around the spectral peak, i.e., the spectral bandwidth is gradually reduced. Herein we define the spectral bandwidth as $\Delta k/k_p$, where $\Delta k$ is a measure of the width of the spectrum estimated as the half-width at half-maximum (see Onorato et al., 2001), and $k_p$ is the peak wavenumber. Since the spectrum becomes higher and narrower around the spectral peak (i.e., smaller $\Delta k/k_p$) if $\gamma$ is increased, four different values of the peak enhancement factor have been used: $\gamma = 1$, 2, 3.3, and 5. The corresponding values of $\alpha$ are then chosen so that $H_s = 6.50\,\mathrm{m}$.

As the dominant wavelength and significant wave height do not change, the wave steepness remains constant: $k_p a = 0.13$, where $a$ is half the significant wave height. We have chosen spectral densities with such a steepness, because, if calculated with respect to a mean wavelength ($\lambda_m = gT_{m_{-10}}/\sqrt{gk}$, where $T_{m_{-10}}$ is a spectral mean period), it represents the upper bound of the joint distribution of significant wave heights and mean wave periods, which were observed during some 270 ship accidents reported as being due to bad weather conditions (Toffoli et al., 2005). It is important to note, furthermore, that the spectral bandwidth changes, and hence different values of the BFI, which is related to the modular instability of free wave modes, are consequently taken into account; for computational details of the BFI and its relation to the JONSWAP spectrum see, for example, Onorato et al. (2006). For the chosen peak enhancement factors, the BFI assumes the following values: BFI $= 2k_pa/(\Delta k/k_p) = 0.25$; 0.55; 0.80; 1.10, respectively.

It is important to note that the time evolution of the surface elevation produces changes to the initial spectral shape. Numerical simulations of two-dimensional wave fields performed by Janssen (2003) indicate that there is a considerable broadening of the spectrum. In particular, the evolution of the spectral bandwidth shows, after an initial overshoot, a rapid transition towards an equilibrium value. It follows, therefore, that the spectral shape at the time of the output storage is actually different from the initial spectral shape. As an example, we have measured that the spectral bandwidth, $\Delta k/k_p$, increases about 5% for an initial BFI $= 0.25$, and up to 20% for an initial BFI $= 0.80$. The latter seems to be consistent with the simulations presented by Janssen (2003) for a similar initial degree of nonlinearity.

## 4. Statistical properties of the surface elevation

The most obvious effect of wave nonlinearity is the sharpening of the wave crests and the flattening of the wave troughs. This results in a deviation of the skewness $\lambda_3$ (i.e., the third order moment of the probability density function of surface elevation) from the value expected in a linear wave field ($\lambda_3 = 0$).

For second-order waves, it can be easily verified that the skewness is a function of the wave steepness (see Srokosz and Longuet-Higgins, 1986). It can be written as follows:

$$\lambda_3 = 3\varepsilon, \tag{6}$$

where $\varepsilon = k_p\sqrt{m_0}$, and $m_0$ is the spectral variance.

Simulated second-order bound waves, which were obtained with constant steepness, show that the skewness is approximately equal to 0.19 for all simulated cases. Therefore, no significant effects of the spectral bandwidth were found. This result is in agreement with Eq. (6).

The numerical simulations of the Euler equations (Eqs. (1) and (2)) performed for this study indicate that higher-order effects of bound waves as well as the nonlinear interaction between free modes provide a very limited contribution to the vertical asymmetry of the wave profile. Thus, the asymptotic value of the skewness does not change significantly with the BFI (see Fig. 1); $\lambda_3$ was, in fact, observed to vary from 0.18, for BFI $= 0.25$, to 0.20, for BFI $= 1.10$. These values are thus consistent with the second-order simulations.

Nonlinear effects also result in a deviation of the fourth-order moment of the probability density function, i.e. kurtosis ($\lambda_4$), from the value expected for a Gaussian random process ($\lambda_4 = 3$). Under the narrow-banded approximation, the contribution of bound waves (second and third-order) to the kurtosis can be expressed as follows

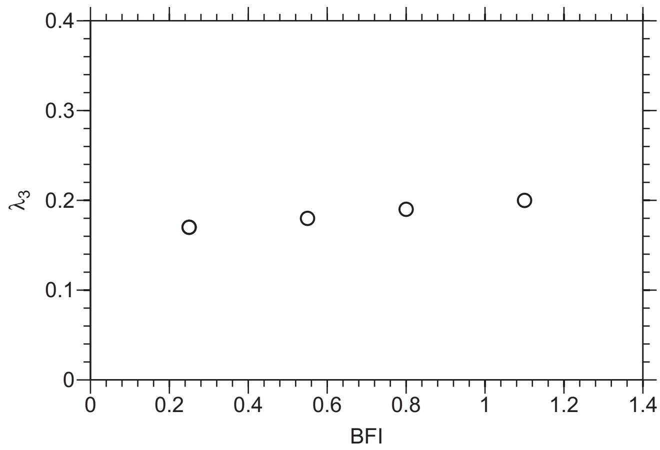


Fig. 1. Skewness ($\lambda_3$) as a function of the BFI: direct simulations of the Euler equations (o).

(see, for example, Mori and Janssen, 2006):

$$\lambda_4 = 24\varepsilon^2. \tag{7}$$

Considering the spectral densities used in this study, Eq. (7) would lead to $\lambda_4 = 3.10$, which is only slightly different than the kurtosis observed in the second-order simulations ($<2\%$). As mentioned in Onorato et al. (2004), however, free waves provide a more relevant contribution to the kurtosis than bound modes if the spectrum is sufficiently narrow. In this respect, when the spectral bandwidth satisfies the conditions $(\Delta k/k_p)^2 < \pi/12\sqrt{3}$, the contribution of free modes, which leads to the modulation instability, dominates the contribution of bound waves (Mori and Janssen, 2006). It follows that for broad-banded spectra (e.g., the case with BFI $= 0.25$ in this study) the modulational instability effects may not be relevant as $(\Delta k/k_p)^2 > \pi/12\sqrt{3}$. The direct simulations of the Euler equations, for this case, show that the value of the kurtosis is in agreement with Eq. (7) as $\lambda_4 = 3.14$. When the BFI increases, however, the modulational instability begins since the spectral bandwidth is reduced. As a result, the occurrence of extreme events becomes more frequent. Thereby, the kurtosis significantly deviates from the value of Eq. (7), and increases as a function of the BFI (see Fig. 2). To some extent, the kurtosis of the simulated profiles is consistent with the theoretical formulation presented by Janssen (2003) and Mori and Janssen (2006), where the kurtosis is calculated as follows:

$$\lambda_4 = \frac{\pi}{\sqrt{3}}\left(\frac{\varepsilon}{\Delta\omega/\omega_p}\sqrt{2}\right)^2. \tag{8}$$

The term within brackets in Eq. (8) corresponds to a slightly different form of the BFI than the one used for this study. It is interesting to note that, for large degrees of nonlinearity (BFI $\geqslant 1.1$), Eq. (8) overestimates the kurtosis of the simulated profiles. This is likely related to the fact that the simulations account for a third order expansion of the vertical velocity only. Nonetheless, our simulations are in agreement with laboratory experiments on

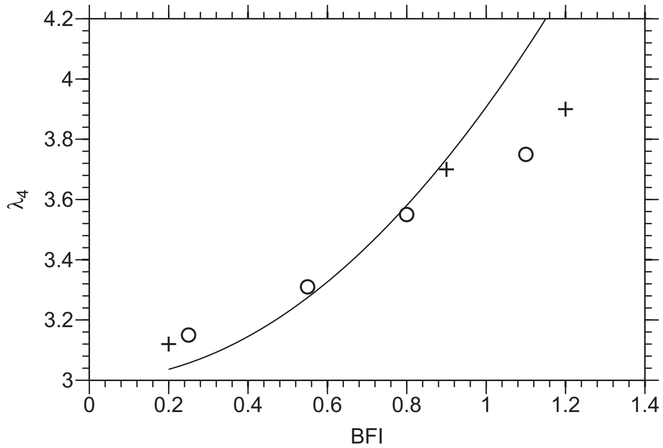


Fig. 2. Kurtosis ($\lambda_4$) as a function of the BFI: theoretical expression (narrow-band wave theory Janssen, 2003; Mori and Janssen, 2006); direct simulations of the Euler equations (o); laboratory experiments (Onorato et al., 2004) (+).

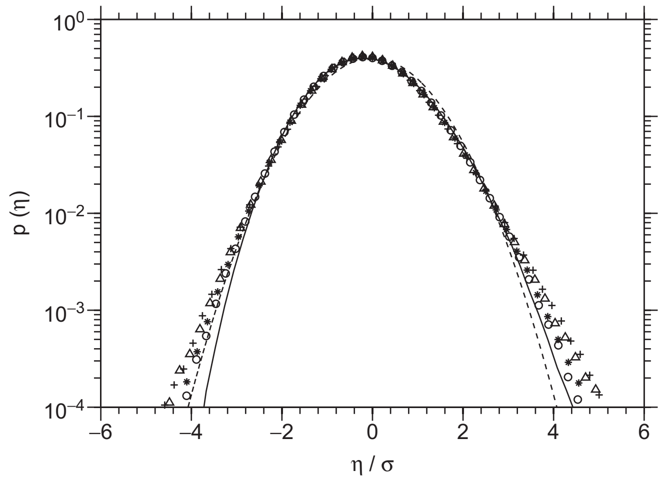


Fig. 3. Probability density function of the surface elevation: normal (Gaussian) distribution (dashed line); Tayfun distribution (Tayfun, 1980) for the surface elevation (solid line); direct simulations (HOSM) from the Euler equations with BFI = 0.25 (o); direct simulations (HOSM) from the Euler equations with BFI = 0.55 (∗); direct simulations (HOSM) from the Euler equations with BFI = 0.80 (△); direct simulations from the Euler equations with BFI = 1.10 (+).

unidirectional wave trains (see Onorato et al., 2004), also for large values of the BFI (see Fig. 2).

It is now instructive to look at the probability density function of the surface elevation. This is presented in Fig. 3, where it is compared with the normal (Gaussian) distribution and a theoretical probability density function for second-order surface elevation (the standard deviation $\sigma$ is here used as a normalizing factor). The latter distribution was first derived by Tayfun (1980); a more user-friendly expression can be found in Socquet-Juglard et al. (2005). The second-order effect, as aforementioned, produces high and sharp crests and shallow and flat troughs. As a result, the tails of the probability density function deviate rightwards from the normal distribution (possible effects due to the spectral bandwidth will be discussed in the next section). If the Euler equations are used to simulate the sea surface, similar degree of vertical asymmetry can be found (see Fig. 1). However, the tails of the distribution behave differently than in second-order wave theory. Whereas the upper tail deviates rightwards as the crests become higher, the lower tail shows that the troughs are actually deeper than for second-order profiles. In particular, the lower tail relaxes on the normal probability density function for relatively low values of the BFI (BFI = 0.25 and 0.55). As the BFI increases, furthermore, the troughs appear to be deeper than in linear wave theory; the lower tail, in fact, deviates leftwards from the Gaussian distribution.

## 5. Probability distribution of the wave amplitude

### 5.1. Theoretical distribution for second-order wave amplitudes

In the case of a narrow-banded spectrum in water of infinite depth, the second-order surface elevation can be written as follows:

$$\eta(x,t) = a(x,t)\cos(\theta) + \tfrac{1}{2}k_p a^2(x,t)\cos(2\theta), \tag{9}$$

where $\theta = k_p x - \omega t + \varepsilon$ and $a(x,t)$ is the slowly varying envelope. The second term on the right-hand side of Eq. (9) generates the Stokes-type contribution, which is a high frequency signal with a local maxima for each crest and trough. It is therefore straightforward to show that the wave crest amplitude assumes the following expression:

$$\eta_c = a + \tfrac{1}{2}k_p a^2. \tag{10}$$

Similarly, the wave trough can be written as follows:

$$\eta_t = a - \tfrac{1}{2}k_p a^2. \tag{11}$$

Under the hypothesis that linear wave amplitudes are Rayleigh distributed, Eq. (10) can be used to derive an expression for the exceedance probability of the crest amplitudes (see Tayfun, 1980, for details); the exceedance probability can be written as follows:

$$P(\eta_c > \eta) = \exp\left[-\frac{8}{H_s^2 k_p^2}\left(\sqrt{1+2k_p\eta} - 1\right)^2\right]. \tag{12}$$

Similarly, we use Eq. (11) to express the exceedance probability for wave troughs:

$$P(\eta_t > \eta) = \exp\left[-\frac{8}{H_s^2 k_p^2}\left(\sqrt{1-2k_p\eta} - 1\right)^2\right]. \tag{13}$$

Note that Eq. (12) is often referred to as the Tayfun distribution (Tayfun, 1980). In the following, Eqs. (12) and (13) are used as reference to investigate the effect of the spectral bandwidth on the probability distribution of crests and troughs.

### 5.2. Wave crest distribution

In Figs. 4 and 5, we present the exceedance probability for the crest amplitude as simulated from second-order wave theory, Eqs. (3) and (5), and the Euler equations, Eqs. (1) and (2), respectively. The results are compared with the theoretical distribution for narrow-banded, second-order waves (Eq. (12)). For convenience, the crest amplitudes are normalized by a constant wave height equal to four times the standard deviation of the whole sample (i.e., the significant wave height of the input spectrum).

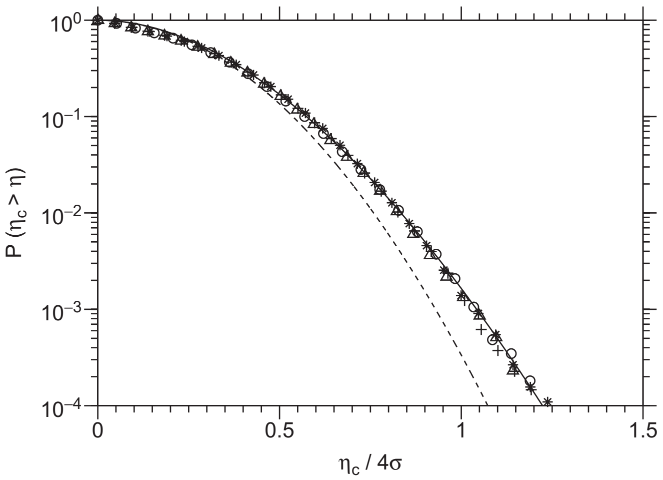


Fig. 4. Wave crest distribution from second-order theory (Eqs. (3) and (5)): Rayleigh distribution (dashed line), second-order theoretical distribution (Tayfun, 1980) (solid line); numerical simulations with $k_pa = 0.13$ and BFI $= 0.25$ (o); numerical simulations with $k_pa = 0.13$ and BFI $= 0.55$ ($*$); numerical simulations with $k_pa = 0.13$ and BFI $= 0.80$ ($\triangle$); numerical simulations with $k_pa = 0.13$ and BFI $= 1.10$ ($+$).

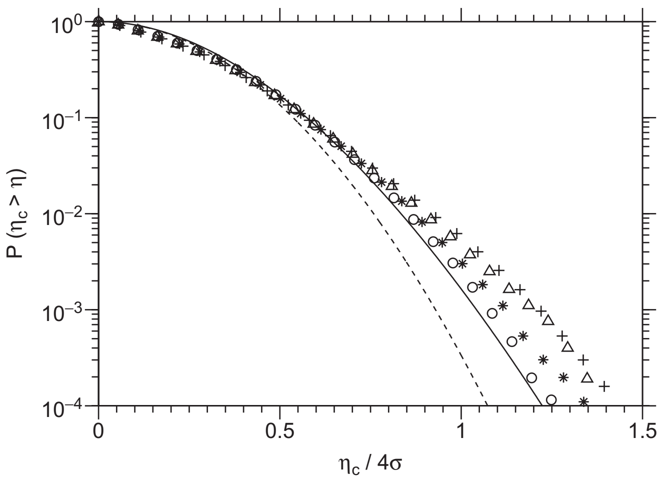


Fig. 5. Wave crest distribution from direct numerical simulations (HOSM) of the Euler equations (Eqs. (1) and (2)): Rayleigh distribution (dashed line), second-order theoretical distribution (Tayfun, 1980) (solid line); numerical simulations with $k_pa = 0.13$ and BFI $= 0.25$ (o); numerical simulations with $k_pa = 0.13$ and BFI $= 0.55$ ($*$); numerical simulations with $k_pa = 0.13$ and BFI $= 0.80$ ($\triangle$); numerical simulations with $k_pa = 0.13$ and BFI $= 1.10$ ($+$).

Note, however, that the wave envelope is modulated due to the sampling variability. This means that the local significant wave height varies. As shown by Bitner-Gregersen and Hagen (2004), this slightly changes the form of the statistical distribution. By using a constant normalizing factor, in this respect, a more conservative result is achieved.

The expression in Eq. (12) indicates that the form of the second-order wave crest distribution only changes according to the wave steepness. Our numerical simulations of irregular second-order wave crests, furthermore, indicate that the shape of this distribution does not significantly change if different spectral bandwidth (and therefore different BFI) are considered. As shown in Fig. 4, in this respect, the Tayfun distribution provides a good estimate of all considered sets of second-order simulations.

If the wave spectrum is broad-banded (for example, the case with BFI $= 0.25$ in this study), the nonlinear interaction between free waves does not have any significant effect on the wave amplitude. As a result, the tail of the wave crest distributions, which were derived from the direct simulations of the Euler equations, only slightly deviates from Eq. (12) (see Fig. 5). The relative difference $\Delta$ between fully nonlinear and second-order crest amplitudes at low probability levels, $P(\eta_c > \eta) \leqslant 0.001$, is almost negligible ($<4\%$ as indicated in Fig. 6). The reason for this departure is most likely related to the effect of third-order bound modes, which slightly modify the kurtosis (cf. Fig. 2). If the wave spectrum is sufficiently narrow, on the other hand, the modulational instability can occur and facilitate the formation of large wave amplitudes. Thus, as the BFI is increased, the form of the statistical distribution changes. Consequently, the departure from the second-order theory becomes more significant; for BFI $= 0.55$, and low probability levels ($P(\eta_c > \eta) \leqslant 0.001$), the crest amplitudes obtained from the simulations of the Euler equations are measured to be 10% higher than second-order crest

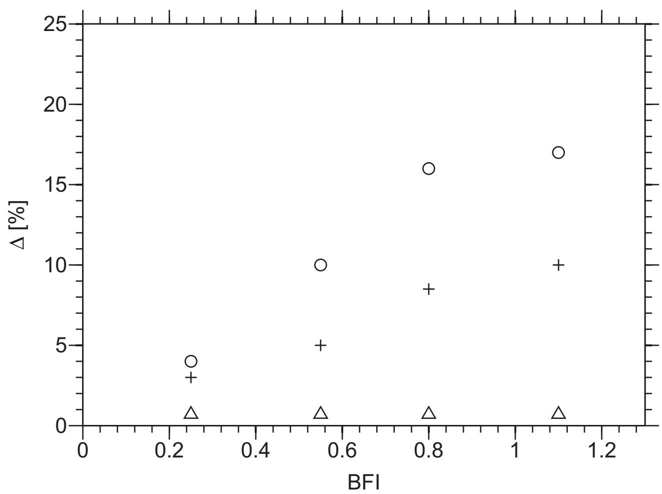


Fig. 6. Relative difference $\Delta$ between wave crests simulated with HOSM and second-order theory at different probability levels: $P(\eta_c > \eta) = 0.1$ ($\triangle$); $P(\eta_c > \eta) = 0.01$ ($+$); $P(\eta_c > \eta) = 0.001$ (o).

amplitudes (Fig. 6); for BFI$\geqslant$0.8, wave crests are about 18% higher than second-order amplitudes. This finding is consistent with the results of flume experiments presented by Onorato et al. (2006). For a practical point of view, it is worth noting that BFI = 0.80 is obtained with a JONSWAP spectral formulation with peak enhancement factor $\gamma = 3.3$, which represents a common spectral shape for many practical applications. The tail of the wave crest distribution, however, does not significantly change further if BFI > 0.80. As shown in Figs. 5 and 6, at low probability levels, $P(\eta_c > \eta) \leqslant 0.001$, the wave crests have approximately the same amplitude for both BFI = 0.80 and 1.10 (cf. Onorato et al., 2006).

It is important to remark that the simulations used for this study only represents unidirectional wave fields. In the more realistic condition of directional sea states, the coexistence of different directional components may limit the effect of the modulational instability and hence reduce the deviation from second-order theory (see, e.g., Onorato et al., 2002; Socquet-Juglard et al., 2005; Gramstad and Trulsen, 2007).

### 5.3. Wave trough distribution

It is relatively well established that the troughs of nonlinear wave profiles are flatter than in a Gaussian random process (see, e.g., Ochi, 1998). Therefore, similarly to what is observed for the wave crests, their statistical distribution is expected to deviate from the Rayleigh density function. Fig. 7, in this respect, shows the theoretical and simulated probability of exceedance for second-order wave troughs in comparison with the Rayleigh distribution. It is interesting to note that the theoretical wave trough distribution, Eq. (13), provides a relatively good estimate of the simulated second-order trough amplitude.

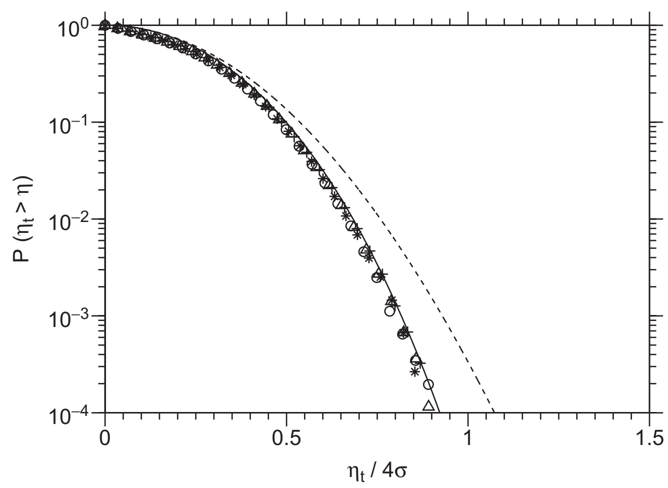


Fig. 7. Wave trough distribution from second-order theory (Eqs. (3) and (5)): Rayleigh distribution (dashed line), second-order theoretical distribution (Eq. 13) (solid line); numerical simulations with $k_pa = 0.13$ and BFI = 0.25 (o); numerical simulations with $k_pa = 0.13$ and BFI = 0.55 ($*$); numerical simulations with $k_pa = 0.13$ and BFI = 0.80 ($\triangle$); numerical simulations with $k_pa = 0.13$ and BFI = 1.10 (+).

Despite the result presented in Fig. 7, direct simulations of the Euler equations of long-crested, wave trains show that troughs can be deeper than in second-order profiles. This is presented in Fig. 8, where their probability of exceedance is compared with the distribution for second-order and linear troughs. As a general result, the wave trough distribution follows the one for second-order profiles if $P(\eta_c > \eta) \leqslant 0.01$. For lower probability levels, however, the wave troughs are deeper than the second-order prediction. For a low value of the BFI (i.e., BFI = 0.25), for example, the trough amplitude can be about 12% deeper (see Fig. 9); the tail of the

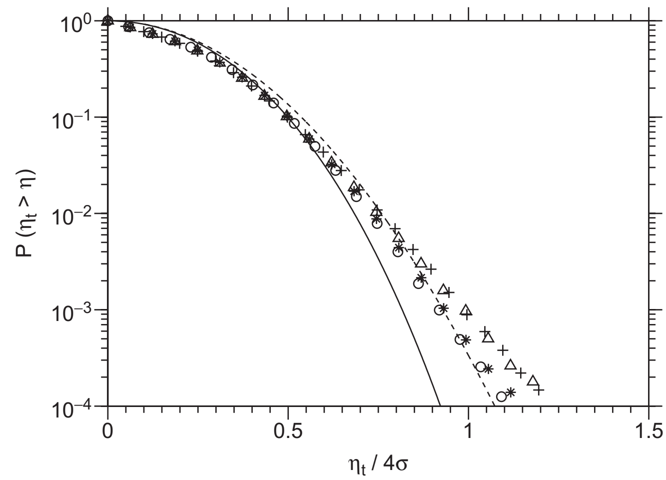


Fig. 8. Wave trough distribution from direct numerical simulations (HOSM) of the Euler equations (Eqs. (1) and (2)): Rayleigh distribution (dashed line), second-order theoretical distribution (Eq. 13) (solid line); numerical simulations with $k_pa = 0.13$ and BFI = 0.25 (o); numerical simulations with $k_pa = 0.13$ and BFI = 0.55 ($*$); numerical simulations with $k_pa = 0.13$ and BFI = 0.80 ($\triangle$); numerical simulations with $k_pa = 0.13$ and BFI = 1.10 (+).

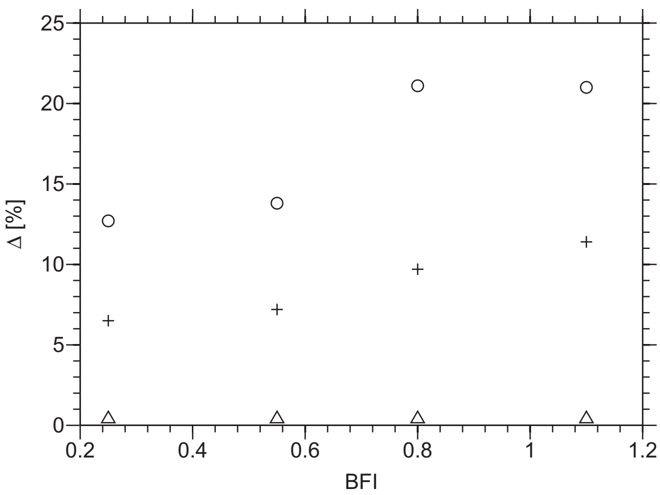


Fig. 9. Relative difference $\Delta$ between wave troughs simulated with HOSM and second-order theory at different probability levels: $P(\eta_c > \eta) = 0.1$ ($\triangle$); $P(\eta_c > \eta) = 0.01$ (+); $P(\eta_c > \eta) = 0.001$ (o).

distribution results in agreement with the Rayleigh distribution. This difference is even more significant than the one observed for wave crests at the same BFI (cf. Fig. 6). Note, moreover, that for BFI $= 0.25$, the modulation instability should not be relevant. Therefore, this difference might be only due to high-order bound contributions.

As the BFI is increased, the deviation of the wave trough distribution from second-order theory increases. For BFI $= 0.55$, however, this departure is not particularly significant if compared to the case with BFI $= 0.25$. The difference between second-order theory and direct simulations of the Euler equations is, in fact, approximately 14% for $P(\eta_c > \eta) = 0.001$ (Fig. 9). This deviation drastically increases when BFI $\geqslant 0.80$, as the effect of the modulational instability becomes more significant (see Fig. 8). For these cases, the simulations of the Euler equations indicates that wave troughs are about 21% deeper than the ones expected in second-order theory. The tail of the distribution, moreover, shows a significant deviation from the Rayleigh probability density function, which underestimates the simulated troughs.

It is important to remark that the simulations only represent unidirectional wave trains. Field measurements, however, show that the trough distribution can actually be overestimated by the Rayleigh distribution (see Mori et al., 2002) and hence the deviation from second-order theory may not be too large.

Using the nonlinear Schrödinger equation, Osborne et al. (2000) have observed that deep holes can occur before and/or after large crests. For a certain time instant, our simulations of the random sea surface show that deep troughs ($\eta_t/4\sigma \approx 1.0$) can sometime occur together with high crests ($\eta_c/4\sigma > 1.2$); two examples are presented in Fig. 10 (upper left and upper right panels). Nonetheless, on average, the deepest troughs was observed to be uncorrelated to the largest crests amplitudes (examples are presented in Fig. 10, lower left and lower right panels). In this respect, we have observed that deep troughs ($\eta_t/4\sigma > 1.0$) mainly occur with relatively low crests ($\eta_c/4\sigma < 1.0$).

### 5.4. *Trough-to-crest wave height distribution*

In the following section, the wave height distribution is presented. To this end, we define the wave height as the sum of the trough depression and the crest elevation of an individual wave (trough-to-crest wave height), which is defined as the portion of the wave signal between two consecutive zero-downcrossings. The wave height distributions obtained from second-order theory and direct simulations of the Euler equations are presented in Figs. 11 and 12, respectively, and compared with the Rayleigh distribution.

The second-order theory does not have any significant effect on the wave height in comparison to the linear wave theory. Therefore, provided the wave spectrum is narrow banded, its distribution can be approximated by the Rayleigh density function (Tayfun, 1980). For the adopted spectral conditions and definition of wave height, however, Fig. 11 shows that the Rayleigh distribution over predicts the second-order simulations; this overestimation slightly increases with the spectral bandwidth. This result is consistent with the findings presented by Tayfun (1981).

In the previous sections, it has already been discussed that the modulational instability of the wave packages produces a modification of the wave crest and trough

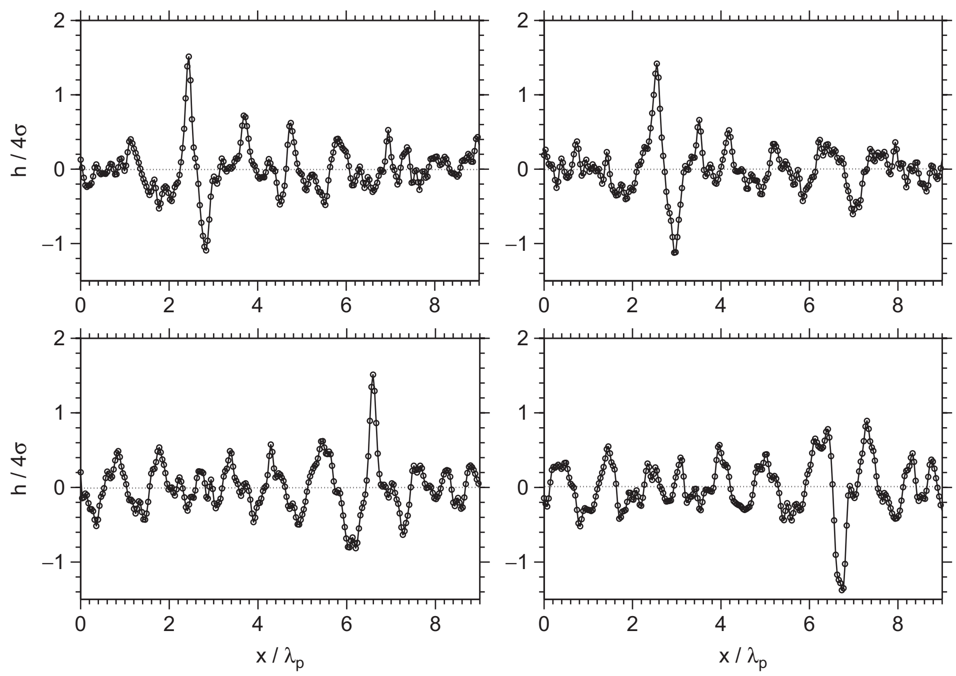


Fig. 10. Examples of nonlinear surface elevation from the Euler equations (BFI = 0.80).

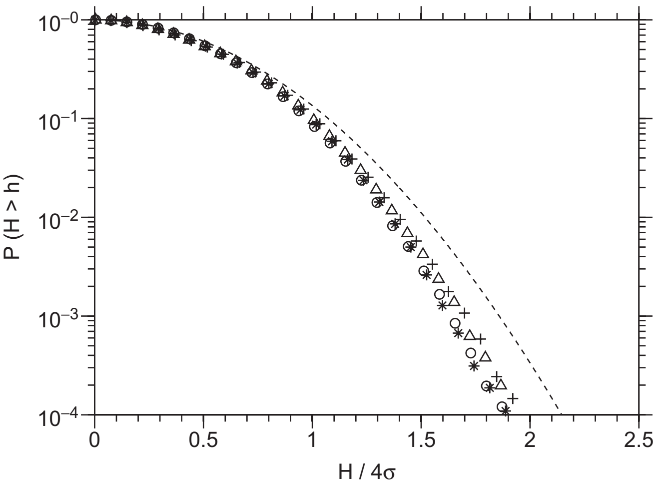


Fig. 11. Trough-to-crest wave height distribution from second-order theory (Eqs. (3) and (5)): Rayleigh distribution (dashed line); numerical simulations with $k_p a = 0.13$ and BFI = 0.25 (o); numerical simulations with $k_p a = 0.13$ and BFI = 0.55 (∗); numerical simulations with $k_p a = 0.13$ and BFI = 0.80 (△); numerical simulations with $k_p a = 0.13$ and BFI = 1.10 (+).

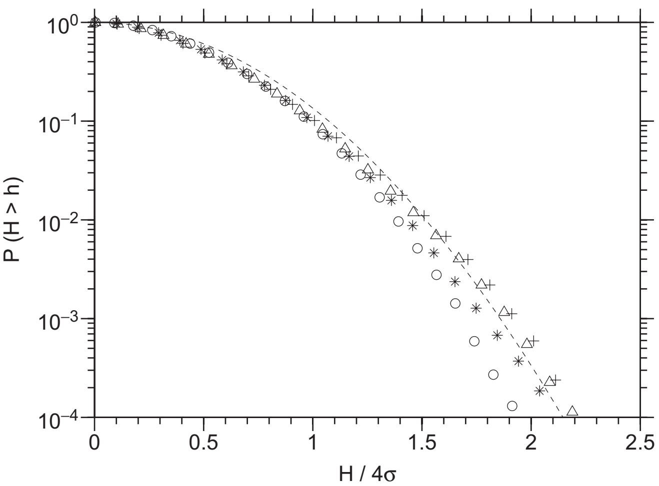


Fig. 12. Trough-to-crest wave height distribution from direct numerical simulation of the primitive Euler equations (Eqs. (1) and (2)): Rayleigh distribution (dashed line); numerical simulations with $k_p a = 0.13$ and BFI = 0.25 (o); numerical simulations with $k_p a = 0.13$ and BFI = 0.55 (∗); numerical simulations with $k_p a = 0.13$ and BFI = 0.80 (△); numerical simulations with $k_p a = 0.13$ and BFI = 1.10 (+).

distribution as there is an excess of extreme values. Consequently, also the form of the wave height distribution is modified. Whereas for low degrees of nonlinearity the difference between second-order theory and the simulations of the Euler equations is limited (<4%, see Fig. 13), for moderate and high degrees of nonlinearity (BFI ⩾ 0.55) the deviation becomes more relevant (>9% at low probability levels). For these conditions, the tail of the distribution is close to the Rayleigh density function. The latter, however, tends to slightly underestimate the simulated heights as BFI ⩾ 0.8 (cf. Mori and Yasuda, 2002). For these degrees of nonlinearity, and

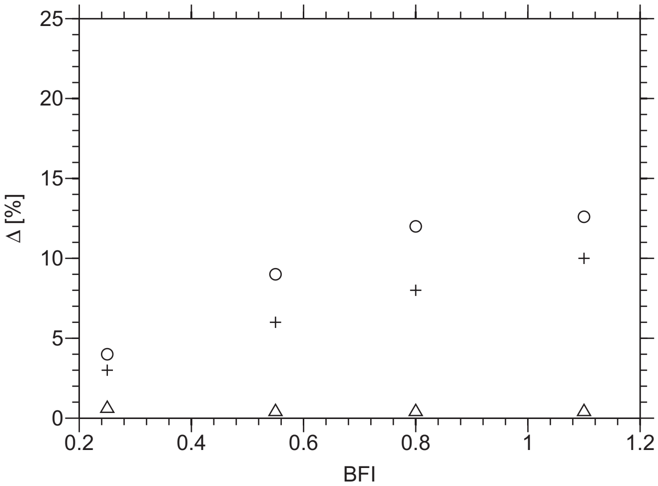


Fig. 13. Relative difference $\Delta$ between trough-to-crest wave heights simulated with HOSM and second-order theory at different probability levels: $P(\eta_c > \eta) = 0.1$ (△); $P(\eta_c > \eta) = 0.01$ (+); $P(\eta_c > \eta) = 0.001$ (o).

low probability levels (0.001), the wave heights are measured to be approximately 13% higher than in second-order theory (see Fig. 13).

### 5.5. Remarks: wave breaking

The numerical models used for this study cannot simulate wave breaking. As the latter may limit the occurrence of very large, steep waves, it may modify the tail of the probability distributions. In a recent work by Babanin et al. (2007), however, it has been shown that wave breaking may not occur when the mean wave steepness of the sea state does not exceed the value of 0.1. In our simulations, the mean steepness ($k_p a = 0.13$) is only slightly higher than this threshold, and hence the wave breaking is expected to occur rarely. Furthermore, using laboratory experiments on regular waves, Babanin et al. (2007) have also shown that deep water waves break when their local steepness exceed 0.44. In this respect, the investigation of the properties of the simulated, individual waves reveals that the local steepness overcomes the value of 0.3 only for a small percentage of them (0.01%). Although wave breaking cannot be excluded a priori, we expect that it does not have a significant effects on the probability distribution reported in Figs. 5, 8, and 12; at least not for the considered probability levels. As the HOSM performs well when the local steepness is lower than 0.3 (see Clamond et al., 2006), furthermore, this may also exclude convergence problems.

## 6. The distribution of extremes

From a practical point of view, it is important to estimate the largest wave amplitude, which is expected to occur within a specific number of observations or an adopted sea state duration (see, for example, Bitner-Gregersen, 2003, where the distribution of extreme crests is discussed in detail by using a second-order wave model). A review concerning the probability distribution of extreme values can be found, for example, in Gumbel (1958), Ochi (1998). In the following, the distribution of extremes is estimated on the basis of a three-parameter Weibull distribution, by which the simulated amplitudes (wave crests, troughs and trough-to-crest heights) are fitted. Assuming, then, that the wave amplitudes are independent events, the occurrence probability for extremes (within a certain number of events) is given by

$$F_E(\eta_e) = \left\{1 - \exp\left[-\frac{\eta_e - \gamma_w}{\alpha_w}\right]^{\beta_w}\right\}^n, \quad (14)$$

where $n$ denotes the number of expected observations, and $\eta_e$ is a generic extreme event; $\alpha_w$ is the scale parameter, $\beta_w$ is the slope, and $\gamma_w$ is the location parameter of the Weibull distribution; they are estimated from the simulated profiles by means of a least square method.

It can be verified that the probability of occurrence for the characteristic largest event, defined as a function of the number of observations, is as follows (see, e.g., Gumbel, 1958):

$$F_E(\eta_{max}) = 1 - \frac{1}{n}. \quad (15)$$

Therefore, considering Eq. (14), an expression for the largest amplitude can be written as

$$\eta_{max} = \gamma_w + \alpha_w[\ln(n)]^{1/\beta_w}. \quad (16)$$

In Figs. 14, 15 and 16 the extreme crests, troughs, and trough-to-crest heights are presented as a function of the number of observations (Eq. (16)). For simplicity, only the cases with BFI = 0.25 and 0.80 are considered as they represent common spectral shape in the design practice ($\gamma = 1.0$ and 3.3, respectively); the distribution for second-order extreme amplitudes is then reported as a reference.

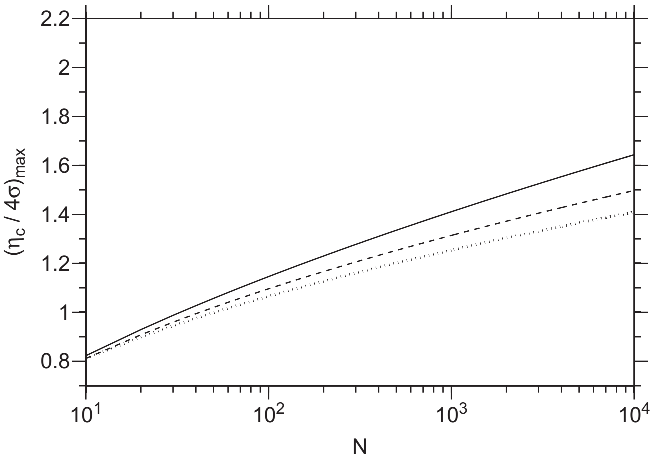


Fig. 14. Extreme crest amplitude as a function of the number of events: second-order (dotted line); direct simulations (HOSM) of the Euler equations with BFI = 0.25 (dashed line); direct simulations (HOSM) of the Euler equations with BFI = 0.80 (solid line).

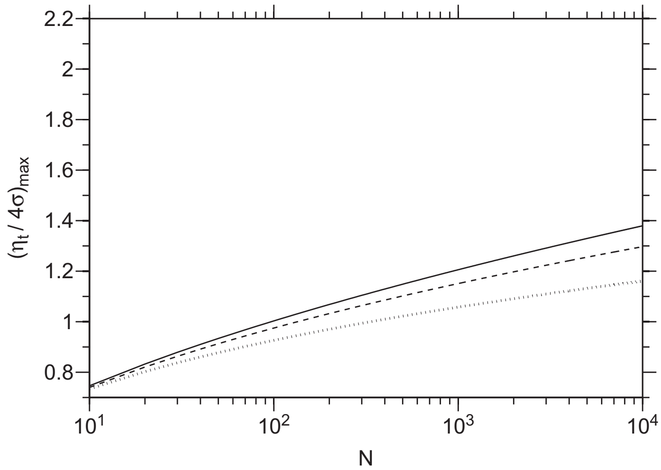


Fig. 15. Extreme trough amplitude as a function of the number of events: second-order (dotted line); direct simulations (HOSM) of the Euler equations with BFI = 0.25 (dashed line); direct simulations (HOSM) of the Euler equations with BFI = 0.80 (solid line).

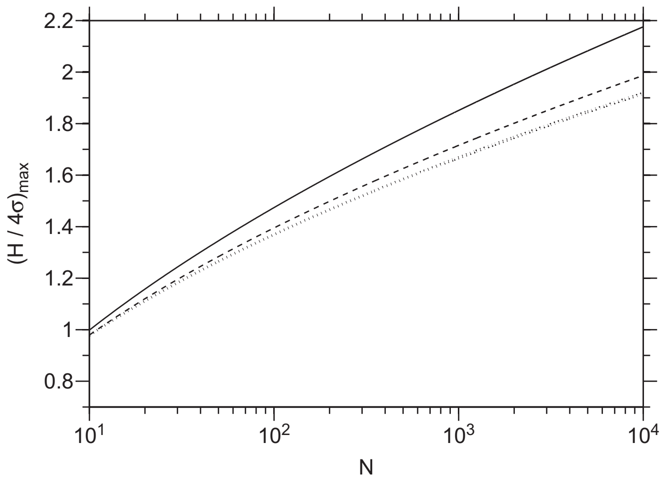


Fig. 16. Extreme trough-to-crest wave height as a function of the number of events: second-order (dotted line); direct simulations (HOSM) of the Euler equations with BFI = 0.25 (dashed line); direct simulations (HOSM) of the Euler equations with BFI = 0.80 (solid line).

The simulations performed herein assume that the sea surface is a stationary random process (i.e., the spectral energy remains constant). In real conditions, this hypothesis is only valid within 20–30 min. Thus, considering that the selected peak period is 10 s, this means a total number of about 150 waves. Within this condition, the second-order wave theory would predict a maximum crest height of about $1.10H_s$ (see Fig. 14). However, if the direct simulations of the Euler equations are taken into account, the maximum crest height may be enhanced up to $1.14H_s$ for BFI = 0.25 and $1.20H_s$ for BFI = 0.80.

It is common practice to consider that the input sea state represents an average description of e.g. a 3-h storm (see, for example, Bitner-Gregersen, 2003). If this is the case, approximately 1000 waves can be expected. Consequently, a second-order wave model would estimate a

Table 1
Extreme values for wave crests, troughs and trough-to-crest heights

| Parameter | Time window | Second-order | HOSM, BFI = 0.25 | HOSM, BFI = 0.8 |
|---|---|---|---|---|
| $\eta_c/4\sigma$ | 150 waves | 1.10 | 1.14 | 1.20 |
| | 1000 waves | 1.25 | 1.31 | 1.41 |
| $\eta_t/4\sigma$ | 150 waves | 0.95 | 1.00 | 1.04 |
| | 1000 waves | 1.06 | 1.15 | 1.21 |
| $H/4\sigma$ | 150 waves | 1.42 | 1.46 | 1.55 |
| | 1000 waves | 1.67 | 1.71 | 1.85 |

maximum crest height of approximately $1.25H_s$, which is the same value obtained from the Euler equations within a number of observations one order of magnitude smaller. From the simulations of the Euler equations, however, the most extreme crest amplitude expected within a 3-h storm could enhance up to $1.31H_s$ if a broad band spectrum is considered (BFI = 0.25). More extreme crests may be encountered if a narrower spectral condition is accounted for (e.g., BFI = 0.80). The maximum crest amplitude may, in these conditions, overcome $1.41H_s$, which is much higher than the crest amplitude of so-called freak or rogue waves (i.e., $1.2-1.3H_s$). The values of the extremes are summarized in Table 1 for completeness.

A similar analysis for the wave troughs indicates that maximum troughs can be equal to the significant wave height within a 30-min time window (Fig. 15) if they are simulated from the Euler equations. Thus troughs are slightly deeper than the second-order wave model predictions. For longer sea state durations (e.g., the 3-h storm condition), the wave trough may be expected to be deeper than $1.21H_s$.

Despite the fact that the crest amplitudes and trough depths reach large values, the trough-to-crest wave heights remain well below twice the significant wave height (see Table 1 and Fig. 16), which also sets a threshold limit for the definition of rogue waves. Within the framework of our numerical approach (i.e., HOSM), such extreme waves could only appear for sea state durations longer than 6 h.

## 7. Conclusions

A series of Monte Carlo simulations have been performed by using second-order wave theory and the primitive Euler equations, in order to analyze the statistical properties of unidirectional, deep water waves. For the simulations of the Euler equations, the high order spectral method proposed by West et al. (1987) has been used. A total of about 60 000 waves have been generated considering different random phases and random amplitudes. Input wave spectra have been chosen in order to have a constant wave steepness and different spectral bandwidth, i.e. different Benjamin-Feir Index.

Whereas the second-order theory only accounts for bound waves, the Euler equations also include the nonlinear interaction between free wave modes, which dominates the non-Gaussian properties of deep water waves. It is important to note, however, that the high order spectral method used for this study is based on a third-order expansion of the vertical velocity.

The analysis of the simulated profiles shows that free waves do not have any significant effect on the vertical asymmetry of the wave profile. However, they may increase the probability of occurrence of extreme events, provided the BFI is sufficiently high. As a result, the tails of the probability density function deviate from the distribution of second-order wave profiles. The wave crests, as expected, are higher than in second-order theory as waves become unstable; for low probability levels, the difference can be up to 18% if BFI $\geqslant$ 0.80.

The instability of wave trains, moreover, has an influence on the wave troughs, which tend to be deeper than in second-order profiles. Using the Euler equations, the troughs have been measured to be about 20% deeper than second-order troughs at low probability levels. In this respect, it is interesting to note that the lower tail of the probability density function of the surface elevation relaxes on the normal distribution for moderate and low values of the BFI; the wave troughs have therefore the same amplitude as a Gaussian random process. Slightly deeper troughs are then to be expected as the BFI increases. In this respect, it is surprising that very deep troughs occur when the BFI is relatively small. Further analysis, however, is needed to reach a firm conclusion.

Although crests and troughs show strong deviations from the second-order theory, we have observed that, for the trough-to-crest height, this deviations is not too large. It is worth noting, in this respect, that for large degrees of nonlinearity, the trough-to-crest wave height simulated from the Euler equations is only slightly underestimated by the Rayleigh probability density function, and it exceeds the second-order prediction of about 13%.

The numerical approach used for this study does not consider wave breaking. Therefore, it cannot be excluded a priori that some simulated large, steep waves may not exist in a natural environment. A recent study on regular waves (Babanin et al., 2007), however, has shown that deep water waves break when the local steepness exceed 0.44. As the waves accounted for our analysis seldom overcome a local steepness of 0.3, we expect that the wave breaking may not influence the main conclusions.

It is important to remark that results based upon the third order truncation in the HOSM do not describe ‘‘fully’’ nonlinear waves; therefore, they must be interpreted within the framework of the numerical approach. Furthermore, only unidirectional wave trains have been taken into account. Real waves, however, are characterized by a certain directional distribution, which may limit the effect of the nonlinear interaction between free wave modes (see, e.g., Onorato et al., 2002; Socquet-Juglard et al., 2005; Gramstad and Trulsen, 2007). Note, however, that strong deviations from the second-order theory have been observed herein for a sea state characterized by a JONSWAP spectrum with peak enhancement factor of 3.3, which is a common spectral shape for many practical applications. Thus, in the case that narrow directional conditions occur, such as swell dominated wave fields, deviations from second-order predictions might be expected.

## Acknowledgments

This work was carried out in the framework of the E.U. project SEAMOCS (contract MRTN-CT-2005-019374). We are thankful to Jason McConochie of Woodside Energy Ltd, Western Australia for his comments on industrial applications of the wave trough probability distributions. The authors are grateful to the anonymous reviewers of this paper for their valuable comments and suggestions, which have helped to improve the presentation of this work.

## References

Annenkov, S.Y., Shrira, V.I., 2001. Numerical modeling of water-wave evolution based on the zakharov equation. Journal of Fluid Mechanics 449, 341–371.

Babanin, A., Chalikov, D., Young, I., Savelyev, I., 2007. Predicting the breaking onset of surface water waves. Geophysics Research Letters 34 (L07605).

Babanin, A.V., Soloviev, Y.P., 1998. Field investigation of transformation of the wind wave frequency spectrum with fetch and the stage of development. Journal of Physical Oceanography 28, 563–576.

Bitner-Gregersen, E., 2003. Sea state duration and probability of occurrence of a freak wave. In: Proceedings of the 22nd International Conference on Offshore Mechanics and Arctic Engineering (OMAE). Cancun, Mexico, June 8–13, 2003.

Bitner-Gregersen, E., Hagen, Ø., 2004. Freak wave events within the second order wave model. In: Proceedings of the 23rd International Conference on Offshore Mechanics and Arctic Engineering (OMAE). Vancouver, Canada, June 20–25, 2004.

Bitner-Gregersen, E., Magnusson, A.K., 2004. Extreme events in field data and in a second order wave model. In: Proceedings of Rogue Waves 2004, Brest, France, October 20–32, 2004.

Brandini, C., 2001. Nonlinear interaction processes in extreme wave dynamics. Ph.D. thesis, Universitá Di Firenze.

Clamond, D., Grue, J., 2001. A fast method for fully nonlinear water-wave computations. Journal of Fluid Mechanics 447, 337–355.

Clamond, D., Francius, M., Grue, J., Kharif, C., 2006. Long time interaction of envelope solitons and freak wave formations. European Journal of Mechanics B/Fluids 25, 536–553.

Dommermuth, D.G., Yue, D.K., 1987. A high-order spectral method for the study of nonlinear gravity waves. Journal of Fluid Mechanics 184, 267–288.

Forristall, G., 2000. Wave crests distributions: observations and second-order theory. Journal of Physical Oceanography 30, 1931–1943.

Gibson, R.S., Swan, C., Tromans, P.S., 2007. Fully nonlinear statistics of wave crest elevation calculated using a spectral response surface method: application to unidirectional sea states. Journal of Physical Oceanography 379, 3–15.

Gramstad, O., Trulsen, K., 2007. Influence of crest and group length on the occurrence of freak waves. Journal of Fluid Mechanics 582, 463–472.

Gumbel, E.J., 1958. Statistics of Extremes. Columbia University Press, New York.

Hasselmann, K., 1962. On the non-linear energy transfer in a gravity-wave spectrum. Part I: General theory. Journal of Fluid Mechanics 12, 481–500.

Janssen, P.A.E.M., 2003. Nonlinear four-wave interaction and freak waves. Journal of Physical Oceanography 33 (4), 863–884.

Komen, G., Cavaleri, L., Donelan, M., Hasselmann, K., Hasselmann, H., Janssen, P., 1994. Dynamics and Modeling of Ocean Waves. Cambridge University Press, Cambridge.

Longuet-Higgins, M., 1963. The effect of non-linearities on statistical distribution in the theory of sea waves. Journal of Fluid Mechanics 17, 459–480.

Longuet-Higgins, M.S., 1952. On the statistical distribution of the heights of sea waves. Journal of Marine Research 11, 1245–1266.

Mori, N., Janssen, P.A.E.M., 2006. On kurtosis and occurrence probability of freak waves. Journal of Physical Oceanography 36, 1471–1483.

Mori, N., Yasuda, T., 2002. Effects of high-order nonlinear interactions on unidirectional wave trains. Ocean Engineering 29, 1233–1245.

Mori, N., Liu, P.C., Yasuda, T., 2002. Analysis of freak wave measurements in the Sea of Japan. Ocean Engineering 29, 1399–1414.

Ochi, M.K., 1998. Ocean Waves: The Stochastic Approach. Cambridge University Press, Cambridge.

Onorato, M., Osborne, A., Serio, M., Bertone, S., 2001. Freak wave in random oceanic sea states. Physical Review Letters 86 (25), 5831–5834.

Onorato, M., Osborne, A.R., Serio, M., 2002. Extreme wave events in directional random oceanic sea states. Physics of Fluids 14 (4), 25–28.

Onorato, M., Osborne, A., Serio, M., Cavaleri, L., 2004. Quasi-resonant interactions and non-gaussian statistics in long crested waves. In: Proceedings of Rogue Waves 2004, Brest, France, October 20–32, 2004.

Onorato, M., Osborne, A., Serio, M., Cavaleri, L., Brandini, C., Stansberg, C., 2006. Extreme waves, modulational instability and second order theory: wave flume experiments on irregular waves. European Journal of Mechanics B/Fluids 25, 586–601.

Osborne, A., Onorato, M., Serio, M., 2000. The nonlinear dynamics of rogue waves and holes in deep-water gravity wave train. Physics Letters A 275, 386–393.

Petrova, P., Cherneva, Z., Guedes Soares, C., 2006. Distribution of crest heights in sea states with abnormal waves. Applied Ocean Research 28, 235–245.

Prevosto, M., 1998. Effect of directional spreading and spectral bandwidth on the nonlinearity of the irregular waves. In: Proceedings of the Eighth International Offshore and Polar Engineering (ISOPE) Conference, Montreal, Canada, May 24–29.

Prevosto, M., Krogstad, H., Robin, A., 2000. Probability distributions for maximum wave and crest heights. Coastal Engineering 40, 329–360.

Socquet-Juglard, H., Dysthe, K., Trulsen, K., Krogstad, H., Liu, J., 2005. Distribution of surface gravity waves during spectral changes. Journal of Fluid Mechanics 542, 195–216.

Srokosz, M.A., Longuet-Higgins, M., 1986. On the skewness of sea-surface elevation. Journal of Fluid Mechanics 164, 487–497.

Tanaka, M., 2001a. A method of studying nonlinear random field of surface gravity waves by direct numerical simulations. Fluid Dynamics Research 28, 41–60.

Tanaka, M., 2001b. Verification of Hasselmann's energy transfer among surface gravity waves by direct numerical simulations of primitive equations. Journal of Fluid Mechanics 444, 199–221.

Tayfun, A.M., 1981. Distribution of crest-to-trough wave heights. Journal of Waterways, Port, Coastal, and Oceanic Engineering 107 (3), 149–158.

Tayfun, M.A., 1980. Narrow-band nonlinear sea waves. Journal of Geophysical Research 85 C3, 1548–1552.

Toffoli, A., Lefèvre, J., Bitner-Gregersen, E., Monbaliu, J., 2005. Towards the identification of warning criteria: analysis of a ship accident database. Applied Ocean Research 27, 281–291.

Tsai, W.-T., Yue, D.K., 1996. Computation of nonlinear free-surface flows. Annual Reviews in Fluid Mechanics 28, 249–278.

West, B.J., Brueckner, K.A., Jand, R.S., Milder, D.M., Milton, R.L., 1987. A new method for surface hydrodynamics. Journal of Geophysical Research 92 (C11), 11803–11824.

Whitham, G., 1974. Linear and Nonlinear Waves. Wiley Interscience, New York.

Zakharov, V., 1968. Stability of period waves of finite amplitude on surface of a deep fluid. Journal of Applied Mechanics & Technology Physics 9, 190–194.

Zakharov, V.E., Dyachenko, A.I., Vasilyev, O.A., 2002. New method for numerical simulation of a nonstationary potential flow of incompressible fluid with a free surface. European Journal of Mechanics B/Fluids 21, 283–291.